

Asymmetry of the angular distribution of Cherenkov photons of extensive air showers induced by the geomagnetic field

P. Homola^{a,b,c,*}, R. Engel^d, H. Wilczyński^a

^a*H. Niewodniczański Institute of Nuclear Physics, Polish Academy of Sciences, Poland*

^b*University of Siegen, Germany*

^c*University of Wuppertal, Germany*

^d*Institut für Kernphysik, Karlsruhe Institute of Technology (KIT), Germany*

Abstract

The angular distribution of Cherenkov light in an air shower is closely linked to that of the shower electrons and positrons. As charged particles in extensive air showers are deflected by the magnetic field of the Earth, a deformation of the angular distribution of the Cherenkov light, that would be approximately symmetric about the shower axis if no magnetic field were present, is expected. In this work we study the variation of the Cherenkov light distribution as a function of the azimuth angle in the plane perpendicular to shower axis. It is found that the asymmetry induced by the geomagnetic field is most significant for early stages of shower evolution and for showers arriving almost perpendicular to the vector of the local geomagnetic field. Furthermore, it is shown that ignoring the azimuthal asymmetry of Cherenkov light might lead to a significant under- or overestimation of the Cherenkov light signal especially at sites where the local geomagnetic field is strong. Based on CORSIKA simulations, the azimuthal distribution of Cherenkov light is parametrized in dependence on the magnetic field component perpendicular to the shower axis and the local air density. This parametrization provides an efficient approximation for estimating the asymmetry of the Cherenkov light distribution for shower simulation and reconstruction in cosmic ray and gamma-ray experiments in which the Cherenkov signal of showers with energies above 10^{14} eV is observed.

*Corresponding author: Tel.: +48 12 662 8348; fax: +48 12 662 8012.

Email address: Piotr.Homola@ifj.edu.pl (P. Homola)

Keywords:

Extensive air showers, Cherenkov light, geomagnetic field

1. Introduction

Many imaging and non-imaging techniques of observing air showers are based on the detection of the abundant number of photons produced as Cherenkov radiation of the secondary electrons and positrons in these showers (see, for example, [1–5]). Cherenkov light also constitutes an important contribution [6] to the optical signal recorded by fluorescence telescopes built for the observation of air showers above 10^{17} eV [7–10].

With a typical Cherenkov angle of the order of 1° in air, the angular distribution of Cherenkov light around the shower axis reflects the angular distribution of the charged particles, mainly electrons and positrons. A proper estimation of the angular distribution of the Cherenkov light produced at various stages of the shower evolution is important for the reconstruction of the shower observables and, hence, the parameters of the primary particle.

Already Hillas noticed in his pioneering work on Cherenkov light production in electromagnetic showers that the energy and angular distributions of electrons exhibit universality features [11, 12]. He derived compact analytic approximations based on the simulation of showers initiated by photons of 100 GeV. Hadronic showers are subject to much larger fluctuations, limiting the applicability of universality-based approximations to much higher shower energies. Only at energies above $\sim 10^{17}$ eV, the energy, angular, and lateral distributions of electromagnetic particles in hadronic showers can be efficiently described by universal functions of shower age and lateral distance in Molière units, e.g. [13–18].

Based on such approximations several parametrizations of the angular distribution of Cherenkov light have been derived, see [7, 11, 15, 19]. In these studies, the angular distribution of Cherenkov photons is considered as approximately symmetric about the shower axis and the influence of the local magnetic field has been neglected. The effects of the geomagnetic field have been studied so far only for primary photons with energies not larger than 100 GeV [20–22] and a compact parametrization was derived in Ref. [20].

The purpose of this work is the quantification of the expected asymmetry of the Cherenkov light distribution of air showers for a wide range of primary energies, extending up to the highest cosmic ray energies. Using

CORSIKA [23] simulations a parametrization of the angular asymmetry induced by the geomagnetic field is derived for air showers from TeV energies up to the highest energies. Considering different local magnetic field strengths and shower geometries it is discussed under what conditions this asymmetry needs to be taken into account.

Furthermore we show how the asymmetry of the azimuthal distribution of Cherenkov photons varies for different shower parameters and geomagnetic conditions. We replace the commonly used angular distribution of Cherenkov photons, assumed to depend only on the viewing angle to the shower axis, $F(\theta)$, with a more accurate function $F(\theta, \phi)$ that also depends on the azimuth angle in the plane perpendicular to the shower axis. The definition of the angles is shown in Figs. 1 and 2.

Throughout this paper we will use the term *viewing angle* for the angle θ between the trajectory of a Cherenkov photon and the shower axis (see Fig. 1). The azimuth angle ϕ used in this study is the angle between the projection of a Cherenkov photon trajectory onto the plane perpendicular to the shower axis, see Fig. 2, and the projection of the geomagnetic field vector onto this plane, which will be referred to as B_{\perp} .

The Monte Carlo simulations presented throughout this paper were carried out with CORSIKA 6.970 [23]. The high energy interactions were processed with the QGSJET 01 model [24] and particles in low energy ($E < 80$ GeV) were treated with GHEISHA [25]. All the simulations were performed using the US Standard Atmosphere density profile [26]. To optimize the computing time we used the thinning algorithm [27] available in CORSIKA. This algorithm keeps only a fraction of the secondary particles in a shower below an adjustable threshold energy, the so-called thinning level. Only one of the particles of each interaction below this energy threshold is followed and an appropriate weight is given to it, while the other particles are dropped. Although the thinning algorithm introduces additional, artificial fluctuations, it is necessary to apply it to keep the computing times manageable. For the purpose of this study we used the thinning level of 10^{-6} .

The Monte Carlo results produced with CORSIKA were processed with COAST 3.01 with the *rootrack* option [28]. COAST (COsrika dAta access Tools) is a library of C++ routines providing simple and standardized access to CORSIKA data. The option *rootrack* enables histogramming shower particles within user-defined planes perpendicular to the shower axis. For the purpose of this study a few dedicated modifications were introduced into both

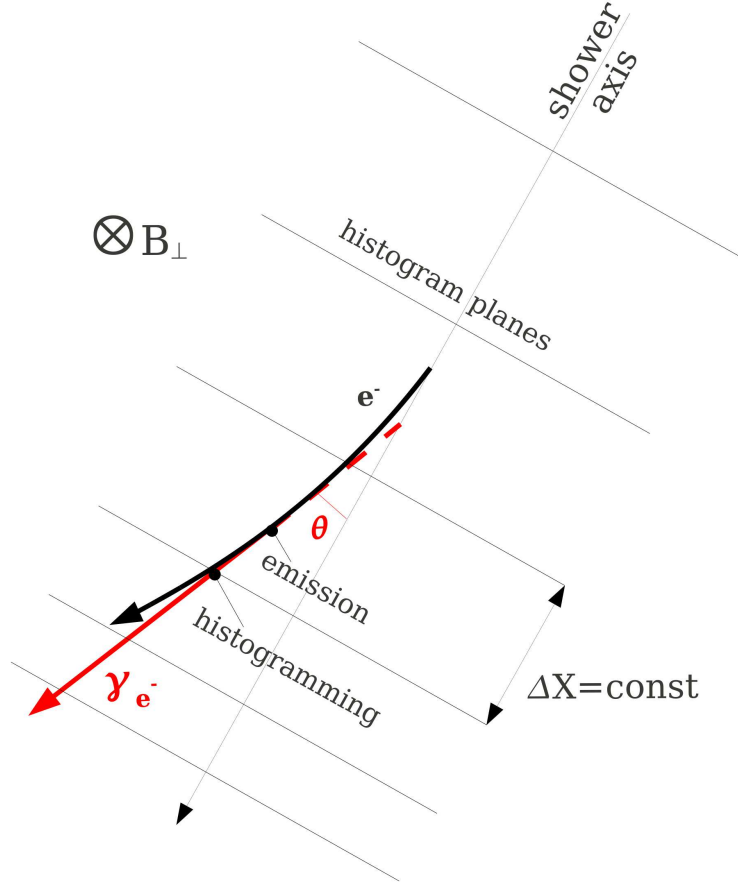


Figure 1: Definition of geometric quantities of relevance to this study. An observer viewing the shower under the angle θ with respect to the shower axis will see the Cherenkov photons as drawn. The viewing angle θ is the angle between the trajectory of a Cherenkov photon and the shower axis, and B_{\perp} denotes the component of the geomagnetic field vector perpendicular to the shower axis. To derive a parametrization the angle of the Cherenkov photons emitted by shower electrons is histogrammed at planes perpendicular to the shower axis. Since we are only interested in the angular distribution of the Cherenkov photons, the lateral distance of the place of their production relative to the shower axis is not considered.

the CORSIKA and COAST codes to enable histogramming of Cherenkov photons. All the shower simulations used for deriving the parametrization were made with 40 observational levels (planes perpendicular to the shower axis) spaced by a constant atmospheric depth interval $\Delta X = 25 \text{ g/cm}^2$ (see

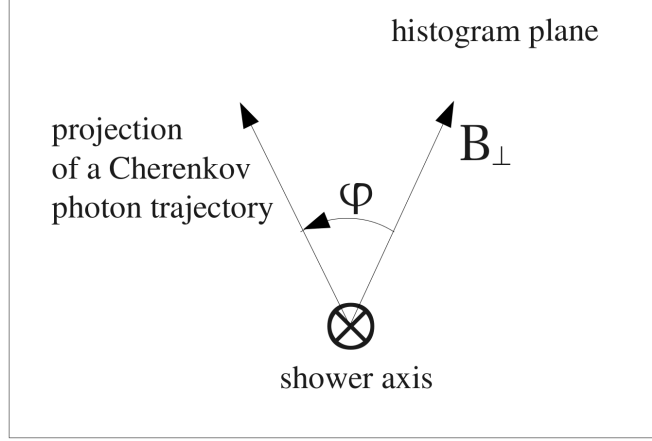


Figure 2: The view of the plane in which the Cherenkov photons are histogrammed. The azimuth angle ϕ used within this document is the angle between B_{\perp} and the projection of a Cherenkov photon trajectory onto the plane perpendicular to the shower axis. The angle ϕ is measured counter-clockwise starting from B_{\perp} .

Fig. 1). The width of the binning in θ is 2° , while the bin width of the azimuth ϕ is 10° .

With use of the above tools we have developed an efficient parametrization that can be used at an arbitrarily selected experimental site if the local geomagnetic field vector is known. As an example, the location of the Tunka experiment [3] ($51^{\circ} 48' \text{ N}$, $103^{\circ} 04' \text{ E}$) is considered in the following. In this experiment a surface array of non-imaging photon detectors is used to record the Cherenkov light emitted by extensive air showers of energies between 10^{14} eV and 10^{18} eV . With the geomagnetic field being exceptionally strong at the Tunka site ($B = 0.6 \text{ G}$), it is well-suited to verify the results of this study experimentally. Even though the angular distribution of the photons cannot be measured directly with the Tunka detectors, it can be derived straightforwardly from the measured lateral distribution of the Cherenkov light at ground.

2. Cherenkov radiation in extensive air showers

Cherenkov radiation in air showers is emitted by charged secondaries traveling with velocity larger than the speed of light in the surrounding medium.

There are three physical parameters important for the overall characteristics of Cherenkov light production, namely (a) the threshold energy of the charged particle above which the Cherenkov radiation is emitted (E_T , for altitudes below 15 km $E_T = 30 - 50$ MeV), (b) the number of produced photons per unit track length of a charged particle, and (c) the angles of their emission. All these quantities depend on the index of refraction n of the medium (i.e. air), and n in turn depends on the local density of the air, $n = n(\rho)$. The dependence of n on the wavelength λ is negligible in the typical λ range of interest for air Cherenkov and fluorescence experiments ($\lambda = 300 \dots 400$ nm) [29].

The angular distribution of the Cherenkov light emitted at angles larger than a few degrees with respect to the shower axis is directly related to the angular distribution of e^\pm in the shower since the typical Cherenkov angles of less than 1° are negligible at such angular scales. In terms of air shower parameters, the angular distribution of Cherenkov light should therefore depend mainly on the angular distribution of charged particles due to multiple scattering, on the local magnetic field strength perpendicular to the trajectory of the particles, and on the air density at the emission point.

2.1. Universality of electron and Cherenkov photon distributions

There have been many studies of universality features of high-energy air showers, see, for example, [13–18]. In these studies it has been shown that most distributions of the bulk of the secondary particles can be described by universal functions depending only on a small number of scaling parameters. Regarding distributions related to the longitudinal shower evolution, the most important parameter is the *shower age* s . The definition of shower age follows from the analytic treatment of electromagnetic cascades [30] and applies only to electromagnetic showers. To extend the concept to showers in general, it is common to use the phenomenological definition [12]

$$s = \frac{3}{1 + 2X_{\text{max}}/X}, \quad (1)$$

where X is the atmospheric slant depth in g/cm^2 and X_{max} is the slant depth of shower maximum.

In the following we only illustrate the universality of relevant particle distributions in air showers by showing the angular distribution of electrons for different energy intervals and different primary particles, including primary

photons (Fig. 3). The simulated distributions were obtained for a vanishing geomagnetic field strength and the histograms were smoothed to provide a better distinction between the electrons of different energy ranges. Each curve corresponds to one shower for each of the primary particles. As expected, the comparison of the curves in Fig. 3 shows no significant differences of the angular distributions of electrons of energies of relevance to Cherenkov light production. The differences found for the higher energy ranges are related to shower-to-shower fluctuations and statistical fluctuations due to the limited number of particles in these histograms. These differences are unimportant for this study as the low-energy electrons are much more abundant and, hence, dominate the expected Cherenkov signal.

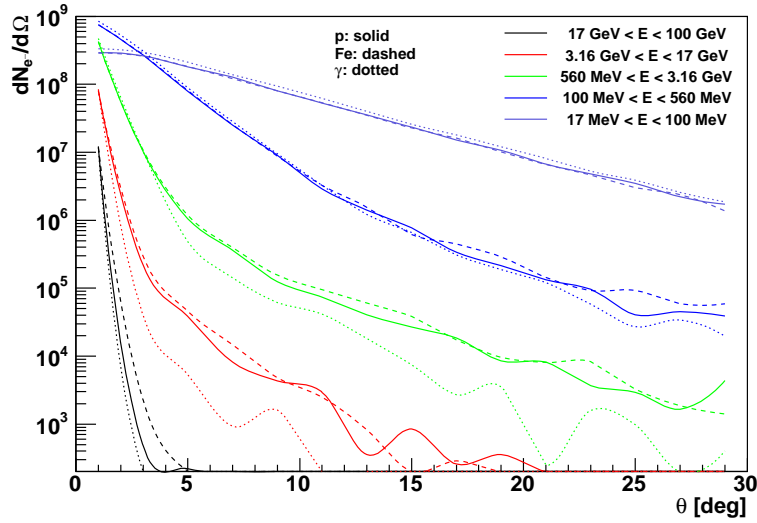


Figure 3: Angular distribution of electrons in three vertical showers induced by a primary proton, iron nucleus, and photon of energies 10^{18} eV for a vanishing geomagnetic field. The distributions are shown at a depth corresponding to the maximum shower size (shower age $s = 1$).

Averaged over azimuth angle, the angular distribution of electrons in showers of 10^{17} eV or higher does not depend significantly on s (in the range of $0.7 < s < 1.2$), E_0 nor on the primary type – if the primary is a nucleus (see e.g. [14, 15, 17]).

The universality of the electron angular distribution leads to a similar universality of the angular distribution of Cherenkov photons. Parametrizations of this distribution as a function of shower age and height can be found e.g. in [15] and [19]. These parametrizations are very good approximations of the true angular distribution if the local geomagnetic field component perpendicular to the shower axis is small or if one considers distributions averaged over the azimuthal angle relative to the shower axis.

2.2. Influence of the geomagnetic field

Since trajectories of charged particles in air showers are bent by the geomagnetic field, an azimuthal asymmetry is expected to be present in the angular particle distribution. This asymmetry leads to an asymmetric distribution of the Cherenkov light as well as to an asymmetric lateral distribution of shower particles at ground. The latter is experimentally well established (see, for example, [31]).

The deflection of e^\pm in the geomagnetic field leads to local maxima at two different azimuth angles in the combined electron and positron distribution. One maximum is related to e^- and the other to e^+ . Furthermore, due to the larger number of e^- in a shower in comparison to e^+ (see e.g. [11]), the maximum related to e^- is higher than that of e^+ . In consequence, the azimuthal distribution of Cherenkov light should be similarly asymmetric.

For investigating this asymmetry with simulated showers and deriving a parametrization we will follow the original approach by Hillas [11]. The effective path length x_m , over which the magnetic field typically acts on a charged particle of energy E and angle θ wrt. the shower axis, can be approximated by [11]

$$\langle x_m \rangle = \frac{30w^{0.2}}{(1 + 36 \text{ MeV}/E)} (\text{g/cm}^2), \quad w = 2(1 - \cos \theta)(E/21 \text{ MeV})^2. \quad (2)$$

One obtains $x_m \sim 0.7X_0$ for $E = 100 \text{ MeV}$ and $\theta = 15^\circ$, using $X_0 = 36 \text{ g/cm}^2$ for the radiation length in air. The magnetic path length x_m increases with E and θ , and increased x_m results in a larger asymmetry of azimuthal distributions of charged particles. The expected asymmetry also increases with the size of the geomagnetic field component transverse to the direction of the particle momentum, B_\perp , i.e. the angular distribution will be more elliptical with increasing B_\perp .

How large an asymmetry of the angular distribution of Cherenkov light can arise is illustrated by an example shown in Fig. 4, where the number

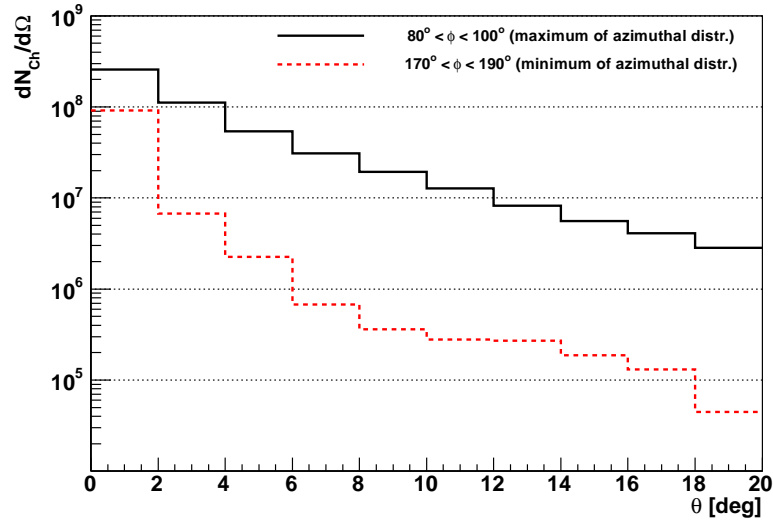


Figure 4: Example of a large asymmetry in angular distributions of Cherenkov photons. The number of Cherenkov photons is shown with respect to the viewing angle for two intervals of the azimuth angle. The first azimuth interval, $80^\circ < \phi < 100^\circ$ (solid black), corresponds to the viewing angles for which the maximum light intensity is observed, while the second interval, $170^\circ < \phi < 190^\circ$ (dashed red), is related to the angles for which the light flux reaches its minimum. The simulation parameters in this example are: proton as primary particle; shower zenith angle 70° ; primary energy 10^{15} eV; observation level is set at $s = 0.8$, corresponding to an altitude of 18 – 20 km; transverse component of the geomagnetic field 0.6 G (compare Fig. 6).

of Cherenkov photons is integrated over two different intervals of azimuth ϕ and shown with respect to the viewing angle θ . The two histograms show the angular distribution of the Cherenkov light for a proton shower of energy $E_0 = 10^{15}$ eV arriving at a zenith angle of 70° . The light emission was observed before the shower reached its maximum development (shower age $s = 0.8$) assuming a geomagnetic field component of $B_\perp = 0.6$ G. The parameters were chosen to maximize the expected asymmetry. The difference in Cherenkov light intensity emitted from the selected regions of the shower observed at different viewing directions exceeds an order of magnitude. For weaker magnetic fields the differences between the maximum and minimum intensities are less pronounced, but still clearly visible.

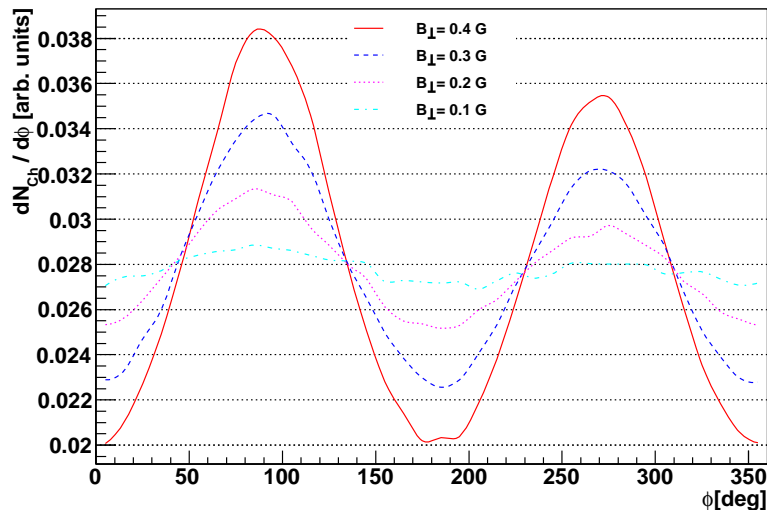


Figure 5: Cherenkov photons in air showers vs. the azimuth angle for $B_{\perp} = 0.1, 0.2, 0.3, 0.4$ G. The simulation parameters in these examples are: proton primaries, shower zenith angle = 60° , primary energy = 10^{19} eV, observation level at $s = 1$ (shower maximum, corresponding to an altitude of 8 – 10 km), viewing angle $8^{\circ} < \theta < 10^{\circ}$.

Some representative examples of azimuthal distributions of Cherenkov photons for fixed viewing angle and varying B_{\perp} are shown in Fig. 5. The left peak of the Cherenkov distributions is related to deflected electrons and the right one to positrons. The electron peak is higher than the positron one due to the 20 – 30% excess of electrons in the shower disk (see e.g. [11, 32]). The peak heights of the distributions shown in Fig. 5 and the asymmetry in Fig. 4 are different because of different altitudes at which the Cherenkov light is produced. A higher air density leads to shorter trajectories of electrons and positrons and correspondingly less geomagnetic deflection.

Figs. 4 and 5 confirm that a parametrization properly describing the angular distribution of Cherenkov light should include a term for the dependence on the azimuthal angle ϕ in the plane perpendicular to the shower axis. Accounting only for the dependence on the viewing angle θ may not be a good approximation in all cases.

3. Parametrization of azimuthal Cherenkov light distribution

Universality of the underlying electron and positron distributions implies that the azimuthal profiles of Cherenkov photons can also be described by a universal function if expressed in suitable variables. Following Elbert *et al.* [20], we make the ansatz that the asymmetry of the azimuthal profile of Cherenkov photons can be approximated by a function of the azimuth angle ϕ , the viewing angle θ , and the parameter a defined as

$$a = B_{\perp}/\rho, \quad (3)$$

where ρ is the local density of air. A dependence on the air density is expected due to the interplay between the magnetic track length x_m , see Eq. (2), and multiple Coulomb scattering. In addition the energy threshold for Cherenkov emission depends on the air density through the density dependence of the refractive index $n = n(\rho)$. Applying the parametrization of $n(\rho)$ as implemented in CORSIKA we neglect the variation of n with wavelength.

In the following we consider proton, nuclei, and photon induced showers in the energy range $10^{15} \text{ eV} < E_0 < 10^{17} \text{ eV}$ and focus on shower ages $0.7 < s < 1.2$, which are of relevance to shower detection.

For the purpose of deriving a parametrization of the azimuthal distributions of Cherenkov photons, we simulated proton-induced showers with three primary energies (10^{15} , 10^{16} and 10^{17} eV) arriving at two different zenith angles (58° and 70°) for different values of B_{\perp} (0.2, 0.3, 0.4, 0.5, and 0.6 G). These simulation parameters were selected to cover a reasonably wide range of the parameter a and to ensure acceptable computing time for producing the shower library.

Of the 40 observation levels, the first of them is always located at the top of the atmosphere which corresponds to a vertical height of 100 km in CORSIKA. To obtain an azimuthal distribution of the emitted Cherenkov radiation for segments of the shower, we fill photons emitted between the two adjacent observational planes in histograms for different viewing angles θ . For each combination of primary energy, arrival direction, and B_{\perp} , a simulation run for a single primary particle was repeated 10 times with different random seed initialization. All the resulting azimuthal distributions of Cherenkov photons shown within this paper are normalized to 1. An example of such a histogram of Cherenkov photons is shown in Fig. 6.

In the next step of the analysis we process each of the selected histograms to find the heights of the peaks related to positrons (B_{e+}) and electrons (B_{e-})

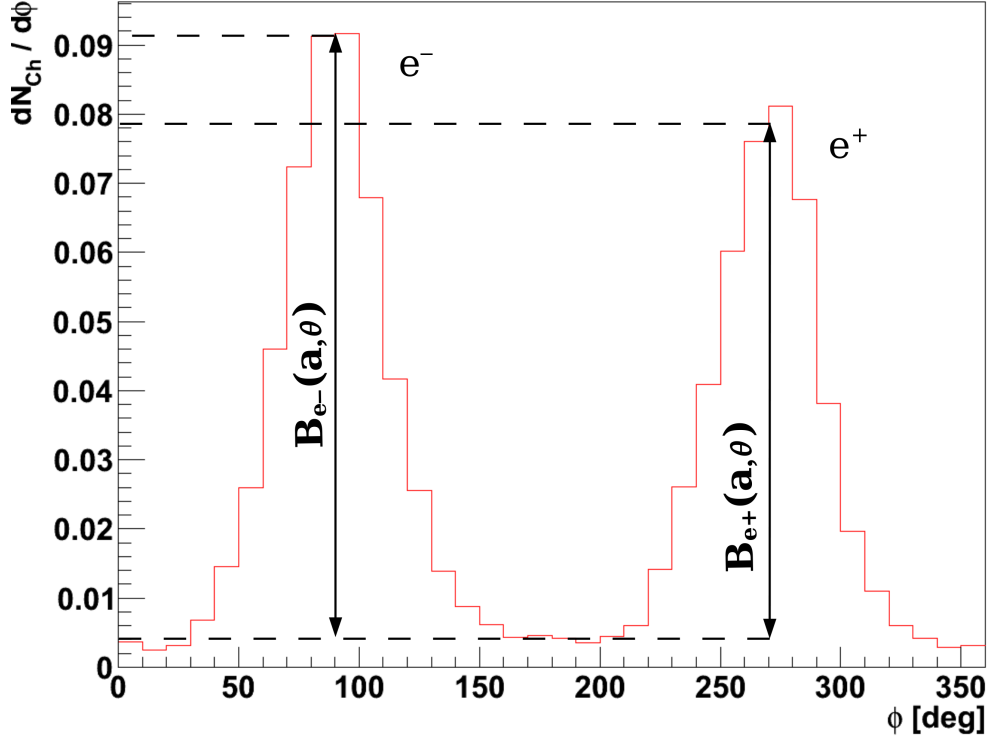


Figure 6: Example histogram of Cherenkov photons from one of the simulations used for deriving the parametrization. The histogram was obtained for a proton primary of 10^{15} eV arriving at a zenith angle of 70° , with $B_\perp = 0.6$ G. Only photons emitted at a shower age $s \approx 0.8$ and viewing angle $14^\circ < \theta < 16^\circ$ are shown. In this case $a = 2.9 \text{ G m}^3 \text{ kg}^{-1}$. See text for details concerning the peak heights B_{e+} and B_{e-} .

(see Fig. 6). The heights are read as the average “maximum” values of the adjacent azimuth bin contents at $80^\circ < \phi \leq 90^\circ$ and $90^\circ < \phi \leq 100^\circ$ for B_{e-} and at $260^\circ < \phi \leq 270^\circ$ and $270^\circ < \phi \leq 280^\circ$ for B_{e+} , subtracting the average “minimum” bin contents at $\phi = 0^\circ$ (bins $350^\circ < \phi \leq 360^\circ$ and $0^\circ < \phi \leq 10^\circ$) and at $\phi = 180^\circ$ (bins $170^\circ < \phi \leq 180^\circ$ and $180^\circ < \phi \leq 190^\circ$), respectively. The values of B_{e+} and B_{e-} depend on a and θ . An example of this dependence is shown in Fig. 7, where B_{e+} is plotted as a function of a for 2 different viewing angles θ . For each histogram of Cherenkov photons an average value of a is calculated based on the atmospheric air density ρ at the two levels determining the histogram, with interpolation of ρ . The maximum uncertainty of this interpolation is reflected in the horizontal error

bars. Fig. 7 indicates that the azimuthal asymmetry increases with a and θ .

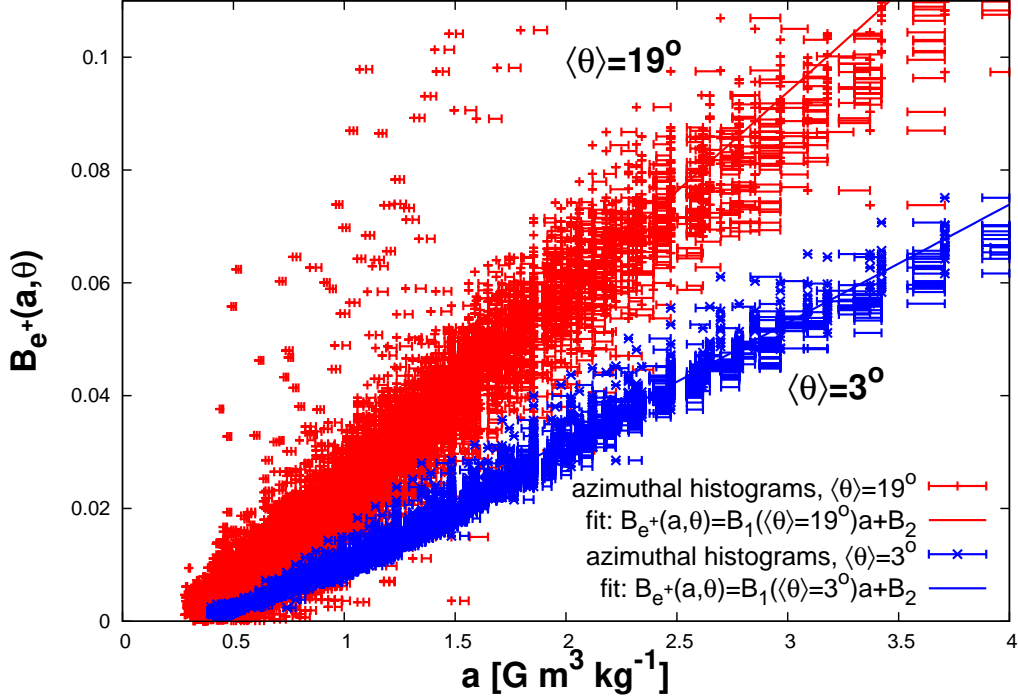


Figure 7: Dependence of peak height $B_{e+}(a, \theta)$ of normalized azimuthal Cherenkov profiles on asymmetry parameter a for different simulation parameters and two different angles θ . The symbols with represent the simulation results used for the fit. The error bars indicate the uncertainty in a resulting from the distance of the different planes for observation. For other details and parameters of the fitted functions, see text.

The increase of B_{e+} with a means that the asymmetry is larger for stronger B_{\perp} or for smaller air density. A stronger B_{\perp} leads to a stronger deflection of the trajectories of charged particles, hence, the asymmetry of the azimuthal profile of Cherenkov photons is more pronounced than in case of weaker B_{\perp} . At the same time the mean free path of electrons over which they are being deflected increases with decreasing air density, which also causes an increase of the azimuthal asymmetry of Cherenkov photons. Finally, the increase of this asymmetry with θ is related to the number of electrons of different energies varying with θ . At larger viewing angles one expects more low-energy electrons. Electrons of low energy are deflected by the geomagnetic field more efficiently than those of higher energies.

From the experimental point of view it is important to keep in mind that, for large viewing angles ($\theta > 20^\circ$), the intensity of the Cherenkov light emitted from the shower particles will become smaller than the Cherenkov light emitted at smaller angles in earlier stages of the shower that is later scattered in the atmosphere to large angles. An investigation of the viewing angle at which the transition between the dominance of direct Cherenkov light and scattered Cherenkov light takes place depends on shower parameters and the observation conditions, and is beyond the scope of this work.

The numerically found values of B_{e^+} and B_{e^-} can be described by a linear function of the parameter a

$$\begin{aligned} B_{e^+/e^-}(a, \theta) &= B_1(\theta)a + B_2 \\ B_1(\theta) &= B_{11}\theta^2 + B_{12}\theta + B_{13}, \end{aligned} \quad (4)$$

where

$$\begin{aligned} B_2(e^+) &= -0.0093 \pm 0.0004 \\ B_{11}(e^+) &= (-6.2 \pm 0.5) \times 10^{-5} \text{deg}^{-2} \\ B_{12}(e^+) &= (0.0022 \pm 0.0001) \text{deg}^{-1} \\ B_{13}(e^+) &= 0.0136 \pm 0.0005, \end{aligned} \quad (5)$$

and

$$\begin{aligned} B_2(e^-) &= -0.0084 \pm 0.0005 \\ B_{11}(e^-) &= (-8.5 \pm 0.5) \times 10^{-5} \text{deg}^{-2} \\ B_{12}(e^-) &= (0.0028 \pm 0.0001) \text{deg}^{-1} \\ B_{13}(e^-) &= 0.0124 \pm 0.0005. \end{aligned} \quad (6)$$

The normalized distribution can be approximated by

$$F(a, \theta, \phi) = A + F_S(a, \theta)[1 + F_A(a, \theta) \sin \phi] \sin^4 \phi, \quad (7)$$

where $A = 1/(2\pi) - 3F_S/8$ is the normalization constant and coefficients $F_S(a, \theta)$ and $F_A(a, \theta)$ are given by the heights of the distribution peaks B_{e^+} and B_{e^-}

$$\begin{aligned} F_S(a, \theta) &= [B_{e^-}(a, \theta) + B_{e^+}(a, \theta)]/2, \\ F_A(a, \theta) &= [B_{e^-}(a, \theta) - B_{e^+}(a, \theta)]/[B_{e^-}(a, \theta) + B_{e^+}(a, \theta)]. \end{aligned} \quad (8)$$

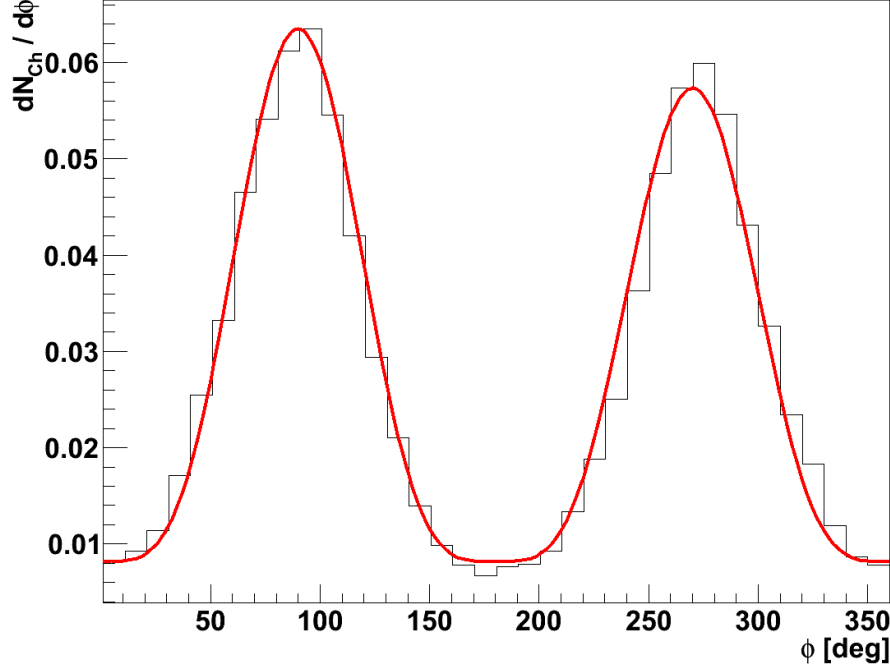


Figure 8: Comparison between an arbitrarily selected azimuthal histogram of Cherenkov photons and the parametrization (7), shown as solid line. The histogram was obtained for an iron primary of energy 10^{17} eV, arriving at a zenith angle of 63° , with $B_\perp = 0.53$ G (corresponding to $a = 1.96$ G m³ kg⁻¹) at viewing angle $10^\circ < \theta < 12^\circ$. The shower age was approximately 0.75.

An example of a shape of the function (7) defined above, for a set of arbitrary parameters, is presented in Fig. 8 in comparison to one shower histogram of Cherenkov photons. The typical shape of the azimuthal distribution of Cherenkov photons, including the excess of electrons in comparison to positrons (i.e. the increased height of the “electron” peak) is well reproduced.

As mentioned earlier, the density of Cherenkov photons decreases rapidly with increasing θ . Therefore the quality of the azimuthal histograms at large viewing angles θ is limited by statistics. Also for small angles θ (near the shower axis), where the phase space due to the small solid angle is substantially reduced, the statistics of Cherenkov photons is insufficient to obtain good quality histograms. As a consequence, the range of the viewing angles

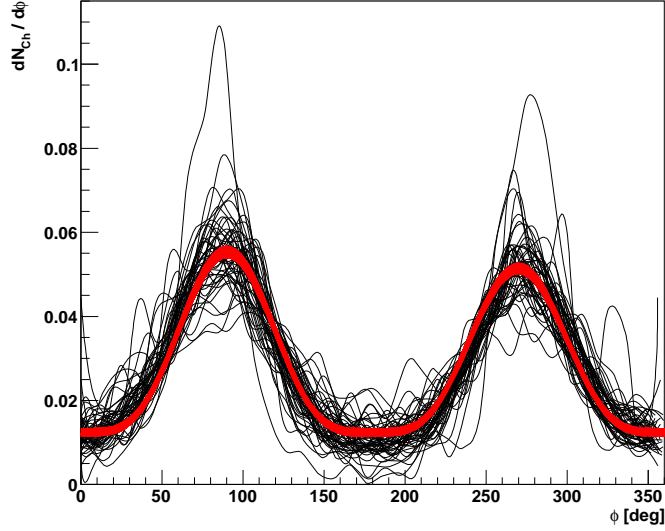


Figure 9: Example of shower-to-shower fluctuations of azimuthal distributions of Cherenkov photons in air showers initiated by primary protons of 10^{14} eV. The thin black lines represent 50 individual air showers and are compared to the parametrization (7) for $a = (1.5 \pm 3\%) \text{ G m}^3 \text{ kg}^{-1}$ and $\langle \theta \rangle = 19^\circ$ (thick red lines).

covered by the presented analysis is limited to $2^\circ < \theta < 20^\circ$.

The parametrization was tested with a set of reference showers generated for the geomagnetic location of the Tunka Cherenkov array. Performing a χ^2 test it is found that about 90% of all simulated histograms deviate less than 30% from the predicted asymmetry for photon-induced showers of primary energies $E_0 \geq 10^{14}$ eV, for showers initiated by protons with $E_0 \geq 10^{15}$ eV, and for iron-initiated showers with $E_0 \geq 10^{16}$ eV. The deviation of a histogram is considered to be less than 30% if the χ^2 , calculated by assuming a 30% uncertainty for each interval of the histogram, is less than unity per degree of freedom. For example, the comparison of 50 histograms of proton-induced showers of 10^{14} eV with the parametrization is shown in Fig. 9. At this low energy, fluctuations lead to significant deviations of individual showers from the parametrization that, by construction, only reproduces the mean distribution.

The shower-to-shower fluctuations are rapidly decreasing with increasing

energy. This improves the overall description of the azimuthal Cherenkov asymmetry, as can be seen in Fig. 10 where proton showers of 10^{17} eV are shown. Deviations between the simulation results and the parametrization are found for the minima of the distribution. It has not been attempted to improve the description in the regions of the minima as one would have to introduce further parameters in Eq. (7).

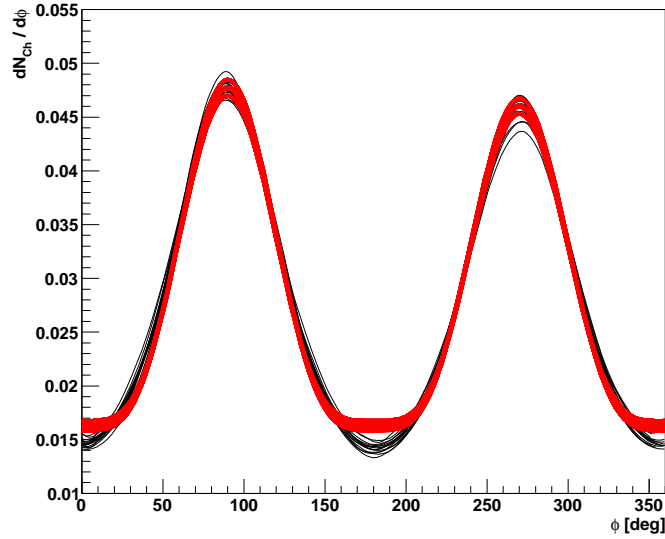


Figure 10: Example illustrating the shower-to-shower fluctuations of azimuthal distributions of Cherenkov photons in air showers initiated by a primary protons of 10^{17} eV. The thin black lines are 9 individual air showers that are compared to the corresponding parametrizations (thick red lines). The parameters of this comparison are $a = (2.0 \pm 3\%) \text{ Gm}^3 \text{ kg}^{-1}$ and $\langle \theta \rangle = 3^\circ$.

In this study, the statistics of histograms are sufficient to confirm the general applicability of the parametrization (7) in the range $0.3 \text{ Gm}^3 \text{ kg}^{-1} < a < 2.5 \text{ Gm}^3 \text{ kg}^{-1}$. This range covers the expected values of a for air shower detectors and air Cherenkov telescopes, see Tab. 1. Asymmetric profiles at small a are less interesting because they can hardly be distinguished from a flat distribution in azimuth.

It is important to note that the precision of the parametrization (7), although satisfactory within the checked range of the parameter a , decreases

Table 1: Examples of values of the parameter a for selected experimental sites, assuming $B_{\perp} = |\vec{B}|$.

experiment	a [Gm ³ kg ⁻¹]			
	10 km a.s.l.	8 km a.s.l.	5 km a.s.l.	3 km a.s.l.
Auger [9]	0.57	0.45	0.33	0.27
H.E.S.S. [33]	0.67	0.53	0.39	0.32
Telescope Array [10]	1.20	0.96	0.70	0.57
Tunka [2]	1.42	1.13	0.82	0.67

with increasing a . Further studies will be needed to extend the parametrization to showers of low energy in the presence of large B_{\perp} . These showers reach their maximum at higher altitudes (smaller ρ) than considered here. It is expected that the peaks in the azimuthal distributions will be narrower under these conditions than the ones predicted by Eq. (7).

4. Summary and outlook

In this work a detailed parametrization of the azimuthal asymmetry of the angular distribution of Cherenkov photons in air showers of energies above 10^{14} has been derived (Eq. 7). The parametrization can be applied to estimate the asymmetry for geomagnetic field strengths and air densities, expressed by the parameter a , in the range $0.3 \text{ G m}^3 \text{ kg}^{-1} < a < 2.5 \text{ G m}^3 \text{ kg}^{-1}$. The wide range in a ensures that an azimuthal asymmetry of Cherenkov photons can be predicted well for the majority of showers of relevant experiments.

The result shows that the asymmetry of the azimuthal Cherenkov distribution caused by the geomagnetic field is expected to be significant when the air density is small and the local magnetic field component transverse to the shower axis is large (large a). The asymmetry increases also with the angle between the viewing direction and the shower axis. Ignoring the asymmetry of the azimuthal distribution of Cherenkov photons can lead to under- or overestimation of the Cherenkov component in the shower light profiles by up to one order of magnitude in the most extreme case.

To illustrate the expected asymmetry for optical air shower observations we consider the ratio $(dN_{\text{ch}}/d\phi)_{\phi=90^\circ}/(dN_{\text{ch}}/d\phi)_{\phi=180^\circ}$ for proton showers

of $10^{18.5}\text{eV}$, arriving at the site of the Pierre Auger Observatory [9] from geographical South at zenith angles of 30° and 60° . If one looks at the depth of maximum of these showers at a viewing angle of 15° the expected asymmetries of the azimuthal Cherenkov light distributions are 1.04 and 1.15, respectively. For $s = 0.8$ the asymmetries are even larger: 1.20 and 1.39. For the Telescope Array site, where the local geomagnetic field is twice as strong as that at the Auger site, the expected asymmetries for showers seen at their maxima at a viewing angle of 15° and arriving at the same zenith angles and from geographical North are 1.45 for 30° and 2.45 for 60° . The respective asymmetries seen at $s = 0.8$ are 1.71 and 3.72.

The results of this work are important for cosmic ray experiments in which the Cherenkov signal of showers is recorded and the local geomagnetic field is not very weak. As the parametrization formulas derived in this paper are applicable also for photon air showers of primary energies down to 100 TeV, they could also be used in the analysis of data of ground-based gamma-ray detectors.

Acknowledgements

This work was partially supported in Poland by the Polish Ministry of Science and Higher Education under grant No. NN 202 2072 38 and by the National Science Centre, grant No. 2013/08/M/ST9/00728, and in Germany by the DAAD, project ID 50725595, the Helmholtz Alliance for Astroparticle Physics and the BMBF Verbundforschung Astroteilchenphysik.

References

- [1] M. Cassidy *et al.*, Proc. of 25th Int. Cosmic Ray Conf., Durban 5 (1997) 189 and arXiv:astro-ph/9707038 [astro-ph].
- [2] B. Antokhonov *et al.* (TUNKA Collab.), Nucl. Instrum. Meth. A628 (2011) 124–127.
- [3] S. Berezhnev, D. Besson, N. Budnev, A. Chiavassa, O. Chvalaev, *et al.* (Tunka Collab.), Nucl. Instrum. Meth. A692 (2012) 98–105 and arXiv:1201.2122 [astro-ph.HE].
- [4] M. Tluczykont, D. Hampf, D. Horns, T. Kneiske, R. Eichler, *et al.*, Adv. Space Res. 48 (2011) 1935–1941 and arXiv:1108.5880 [astro-ph.IM].

- [5] H. J. Völk and K. Bernlöhr, *Exper. Astron.* 25 (2009) 173–191 and arXiv:0812.4198 [astro-ph].
- [6] M. Unger, B. R. Dawson, R. Engel, F. Schüssler, and R. Ulrich, *Nucl. Instrum. Meth.* A588 (2008) 433–441 and arXiv:0801.4309 [astro-ph].
- [7] R. M. Baltrusaitis *et al.* (Fly’s Eye Collab.), *Nucl. Instrum. Meth.* A240 (1985) 410–428.
- [8] J. Boyer, B. Knapp, E. Mannel, and M. Seman, *Nucl. Instrum. Meth.* A482 (2002) 457–474.
- [9] J. A. Abraham *et al.* (Pierre Auger Collab.), *Nucl. Instrum. Meth.* A620 (2010) 227–251 and arXiv:0907.4282 [astro-ph].
- [10] H. Tokuno, Y. Tameda, M. Takeda, K. Kadota, D. Ikeda, *et al.* (TA Collab.), *Nucl. Instrum. Meth.* A676 (2012) 54–65 and arXiv:1201.0002 [astro-ph.IM].
- [11] A. M. Hillas, *J. Phys.* G8 (1982) 1461–1473.
- [12] A. M. Hillas, *J. Phys.* G8 (1982) 1475–1492.
- [13] M. Giller, G. Wieczorek, A. Kacperczyk, H. Stojek, and W. Tkaczyk, *J. Phys.* G30 (2004) 97–105.
- [14] M. Giller, A. Kacperczyk, J. Malinowski, W. Tkaczyk, and G. Wieczorek, *J. Phys.* G31 (2005) 947–958.
- [15] F. Nerling, J. Blümer, R. Engel, and M. Risse, *Astropart. Phys.* 24 (2006) 421–437 and astro-ph/0506729.
- [16] P. Lipari, *Phys. Rev.* 79 (2008) 063001 and arXiv:0809.0190 [astro-ph].
- [17] S. Lafebre, R. Engel, H. Falcke, J. Hörandel, T. Huege, J. Kuijpers, and R. Ulrich, *Astropart. Phys.* 31 (2009) 243–254 and arXiv:0902.0548 [astro-ph.HE].
- [18] M. Ave, R. Engel, J. Gonzalez, D. Heck, T. Pierog, and M. Roth, *Proc. of 31th Int. Cosmic Ray Conf.*, Beijing (2011) #1025.
- [19] M. Giller and G. Wieczorek, *Astropart. Phys.* 31 (2009) 212–219.

- [20] J. W. Elbert, T. Stanev, and S. Torii, Proc. of 18th Int. Cosmic Ray Conf., Bangalore 6 (1983) 227.
- [21] P. M. Chadwick *et al.*, J. Phys. G 25 (1999) 1223.
- [22] S. C. Commichau *et al.*, Nucl. Instrum. Meth. 595 (2008) 572.
- [23] D. Heck, J. Knapp, J. Capdevielle, G. Schatz, and T. Thouw, Wissenschaftliche Berichte, Forschungszentrum Karlsruhe FZKA 6019 (1998) .
- [24] N. N. Kalmykov, S. S. Ostapchenko, and A. I. Pavlov, Nucl. Phys. Proc. Suppl. 52B (1997) 17–28.
- [25] H. Fesefeldt, preprint PITHA-85/02, RWTH Aachen, 1985.
- [26] National Aeronautics and Space Administration (NASA), NASA-TM-X-74335, 1976.
- [27] M. Kobal, Astropart. Phys. 15 (2001) 259–273.
- [28] R. Ulrich, <http://www-ik.fzk.de/~rulich/coast/>, 2011.
- [29] K. Bernlöhr, Astropart. Phys. 30 (2008) 149.
- [30] B. Rossi and K. Greisen, Rev. Mod. Phys. 13 (1941) 240–309.
- [31] P. Abreu *et al.* (Pierre Auger Collab.), JCAP 1111 (2011) 022 and [arXiv:1111.7122](https://arxiv.org/abs/1111.7122) [astro-ph.IM].
- [32] T. Bergmann *et al.*, Astropart. Phys. 26 (2007) 420–432 and [astro-ph/0606564](https://arxiv.org/abs/astro-ph/0606564).
- [33] <http://www.mpi-hd.mpg.de/hfm/HESS/>.